Molecular Mechanism for Converting Carbon Dioxide Surrounding Water Microdroplets Containing 1,2,3-Triazole to Formic Acid

Ke Gong,[§] Yifan Meng,[§] Richard N. Zare,* and Jing Xie*

Cite This: https://doi.org/10.1021/jacs.4c00529

Read Online

ACCESS | 📊 Metrics & More | 📖 Article Recommendations | 🆂🅸 Supporting Information

ABSTRACT: Spraying water microdroplets containing 1,2,3-triazole (Tz) has been found to effectively convert gas-phase carbon dioxide (CO_2), but not predissolved CO_2, into formic acid (FA). Herein, we elucidate the reaction mechanism at the molecular level through quantum chemistry calculations and *ab initio* molecular dynamics (AIMD) simulations. Computations suggest a multistep reaction mechanism that initiates from the adsorption of CO_2 by Tz to form a CO_2-Tz complex (named reactant complex (RC)). Then, the RC either is reduced by electrons that were generated at the air−liquid interface of the water microdroplet and then undergoes intramolecular proton transfer (PT) or switches the reduction and PT steps to form a $[HCO_2$-$(Tz$-$H)]^-$ complex (named PC$^-$). Subsequently, PC$^-$ undergoes reduction and the C−N bond dissociates to generate COOH$^-$ and $[Tz$-$H]^-$ ($m/z = 69$). COOH$^-$ easily converts to HCOOH and is captured at $m/z = 45$ in mass spectroscopy. Notably, the intramolecular PT step can be significantly lowered by the oriented electric field at the interface and a water-bridge mechanism. The mechanism is further confirmed by testing multiple azoles. The AIMD simulations reveal a novel proton transfer mechanism where water serves as a transporter and is shown to play an important role dynamically. Moreover, the transient ●COOH captured by the experiment is proposed to be partly formed by the reaction with H●, pointing again to the importance of the air−water interface. This work provides valuable insight into the important mechanistic, kinetic, and dynamic features of converting gas-phase CO_2 to valuable products by azoles or amines dissolved in water microdroplets.
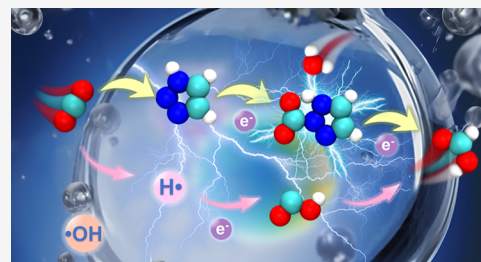
INTRODUCTION

Transforming carbon dioxide (CO_2) to formic acid (FA; HCOOH) is a direct way to alleviate the excess emission of CO_2 in the atmosphere and produce, at the same time, a valuable chemical commodity,[1−3] as well as to create a potential hydrogen storage system.[4] Motivated by these benefits, extensive studies have been carried out.[5−8] Traditionally, formic acid can be formed from CO_2 by using metal catalysts (like Pt, Cu, Co, *etc.*),[9−13] electrochemistry,[14−17] or photochemistry.[18−20] Recently, water microdroplet chemistry has emerged as an alternative approach, for it can accelerate reactions by many orders of magnitude and generate new products.[21−27] Taking advantage of these properties, Song et al. successfully transformed gas-phase CO_2 to formic acid by spraying water microdroplets that contain 1,2,3-triazole (Tz; $C_2N_3H_3$) into CO_2 gas at room temperature.[28] Remarkably, this process did not involve any metal catalysts and was conducted under mild external conditions, thus opening a promising, eco-friendly way to form formic acid.

Experimentally, the authors have confirmed that the CO_2 reduction mainly happens at the gas−water interface of the microdroplet because spraying carbonated water, which contains artificially injected CO_2, does not lead to the formation of formic acid.[28,29] However, a molecular-level mechanism has not yet been definitively established. It has been proposed that the reactions in microdroplets can be affected by several factors,

including partial solvation,[30,31] extreme pH,[32] high interfacial electric field (strength of ∼10^9 V/m),[26,33−36] and orientation of molecules at the interface,[34,37−39] as well as evaporation which increases the reagent concentration.[40] Because the CO_2 conversion process involving proton transfer (PT) is dynamic, it requires a fundamental understanding of its kinetics and dynamics at the air−water interface of the microdroplets. To account for these factors, we present a combined quantum chemistry and *ab initio* molecular dynamics (AIMD) simulation to elucidate the mechanism of Tz-containing microdroplets converting CO_2 in contact with the microdroplet surface to formic acid.

Our calculations reveal the mechanism of the CO_2-to-FA transformation in water microdroplets. The key questions we explored are as follows: (1) What is the order of protonation and reduction? (2) What is the source of proton, Tz, or water molecules? (3) How do above-mentioned factors affect the kinetics of the reaction?, and (4) What is the dynamical role of

Table 1. Multiple Reaction Free Energies ([a]ΔG, kcal/mol), Electron Affinities (EA, kcal/mol), and Reduction Potential (E_{red}, V) as Calculated in the Gas Phase and/or Aqueous Phase

reaction	gas	aqueous	[b]half-solvation
	ΔG_{gas}	$\Delta G_{aq.}$	ΔG_{half}
$COOH^- + H_3O^+ \rightarrow HCOOH + H_2O$	−214.9	−54.3	−135.3
$OH^- + H_3O^+ \rightarrow \bullet OH + H\bullet + H_2O$	−117.1	75.1	−21.6
$CO_2 + H\bullet \rightarrow \bullet COOH$	3.6	−6.3	−2.2
$RC + H\bullet \rightarrow HRC\bullet$	−2.9	−10.5	−7.0
$HRC\bullet \rightarrow \bullet COOH + Tz$	2.3	0.7	2.2
$RC + H\bullet \rightarrow \bullet COOH + Tz$	−0.6	−9.8	−4.8
$CO_2 + H_3O^+ \rightarrow COOH^+ + H_2O$	34.1	39.5	35.3
$CO_2{}^- + H_3O^+ \rightarrow \bullet COOH + H_2O$	−164.4	−8.2	−87.9
$Tz + H_3O^+ \rightarrow HTz^+ + H_2O$	−36.1	−6.2	−32.8
	ΔG_{gas}		[d]$E°_{red}$(V vs SHE)
$CO_2 + e^- \rightarrow CO_2{}^-$	11.5		−1.9 V[61]
$COOH^+ + e^- \rightarrow \bullet COOH$	−187.0		0.29 V
$^\bullet COOH + e^- \rightarrow COOH^-$	−31.1		0.11 V
$Tz + e^- \rightarrow Tz^-$	25.1		−2.99 V

[a]The DLPNO−CCSD(T)/aug-cc-pVTZ//M06-2X/6-31+G(d,p) method and SMD solvent model were used for liquid-phase calculation. Original data are presented in Table S5. [b]half-solvation means half of the solvation energy was added to the gas-phase values. The reduction potential was calculated against SHE.

water molecules at the air−water interface? The simulation results reveal that CO_2 forms a complex with Tz before intramolecular proton transfer and electron reduction. The presence of an interfacial electric field and water molecules effectively promotes the progression of the reaction. A distinct mode of proton transfer at the air−water interface, differing from the proton-shuttle mechanism, has also been unveiled. The role of H$\bullet$ at the surface of the microdroplet was also explored.

This comprehensive computational work sheds light on the important mechanistic and kinetic features of the CO_2-to-FA reaction in a water microdroplet and provides valuable insight into the development of water microdroplet chemistry as greener and cost-effective avenues for CO_2 conversion.[41,42]

METHODS

Mass Spectrometry. All experimental studies were performed using the protocol described in detail in ref 28.

Isomers. 1-H-Tz and 2-H-Tz are isomers of triazole close in energy, and both are mentioned in microdroplet experiments (Scheme S1). We performed calculations for both isomers; the main text focuses on the 1-H-Tz species, and data for 2-H-Tz are provided in the Supporting Information.

Quantum Chemical Calculations. The structures were optimized using the M06-2X functional[43] with a 6-31+G(d,p)[44−50] basis set. Vibrational frequencies were calculated to confirm the nature of stationary points that the minima have no imaginary frequency and transition states (TSs) have one imaginary frequency. Intrinsic reaction coordinate (IRC) calculations were performed on each TS to confirm its minimum energy path. On top of the optimized structures, single-point energy calculations were performed by the DLPNO−CCSD(T)/aug-cc-pVTZ method.[51−53] For aqueous phase calculations (i.e., in bulk solution), a SMD-implicit solvent model was used.[54] We denote it as DLPNO−CCSD(T)/aug-cc-pVTZ//M06-2X/6-31+G(d,p). A benchmark study (Supporting Information) indicates the accuracy of this method.

The standard reduction potential of species A was computed relative to the standard hydrogen electrode (SHE)

$$E°_{rel,SHE}(A|A^-) = -\Delta_r G°_S(A|A^-)/F - E°_{abs}(SHE)$$

where $\Delta_r G°_S$ is the standard reaction free energy of the $A + e^- \rightarrow A^-$ reaction in solution, F is the Faraday constant, and $E°_{abs}$(SHE) is the standard hydrogen electrode potential (4.44 V) at 298.15 K.[55] Calculational details are presented in the Supporting Information.

The effect of an external electric field (EEF) was studied in Gaussian16 with the keyword "Field = M ± N," which defines the EEF axis, its direction, and its magnitude. Here, the M06-2X/6-31+G(d,p) level of theory was used. The field strength (F_x) was allowed to range from $F_x = -0.1$ to 0.1 V/Å; this range is on the order of the electric field observed at the air−water interface of microdroplets.

Except for DLPNO−CCSD(T), single-point calculations were performed using the ORCA 5.0 package.[56] The rest of the quantum chemistry calculations were performed using the Gaussian16 package.[57]

Ab Initio Molecular Dynamics (AIMD). To investigate the dynamic behavior of the reaction with explicit water molecules at the air−water interface, we performed Born−Oppenheimer AIMD simulations with metadynamics-based methods using the CP2K package.[58] The simulations were initiated with the reactant complex (RC). The air−water interface was constructed by placing 100 water molecules in the middle of a cell of $15.0 \times 50.0 \times 15.0$ Å[3] (Figure S8). The AIMD simulation was performed in a canonical ensemble (NVT) using a time step of 1 fs. The temperature was set to 300 K and controlled using a velocity rescaling thermostat. The BLYP-D3 functional used the DZVP-SR-MOLOPT-GTH basis set. The self-consistent field cycle was converged using the orbital transformation method.

The system was first equilibrated for 20 ps with the structure of the RC fixed and the water molecules relaxed. This allows water molecules to orient randomly around the RC. A total of 20 configurations were randomly selected from the equilibration trajectory. Then, stepwise multi-subphase space (SMS) metadynamics[59] were performed for each configuration and each trajectory was simulated for at least 35 ps. The collective variable (CV) is the C−N distance. A more detailed description of AIMD simulations can be found in the Supporting Information.

RESULTS AND DISCUSSION

Overall Mechanism. Converting CO_2 to $COOH^-$ requires one proton and two electrons. The negatively charged C atom in $COOH^-$ can easily gain a proton from H_2O and form formic acid (HCOOH) (see the values in Table 1). Hence, we focus on the formation of $COOH^-$. The source of electron can be derived from the hydroxide anion (OH^-), as the strong electric field at the air−water interface of the microdroplet is proposed to

facilitate the electron transfer and generate ●OH and e⁻.[60] If Tz is the proton donor, the total reaction is

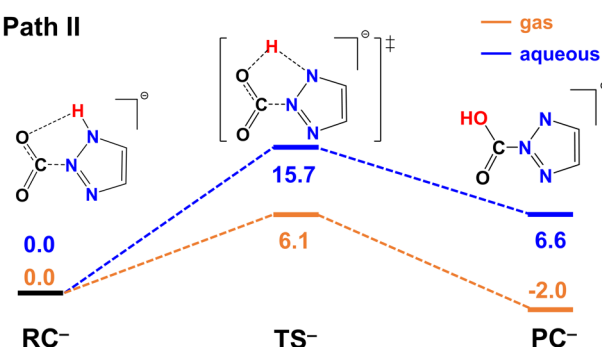$$CO_2 + Tz + 2e^- \rightarrow COOH^- + [Tz\text{-}H]^- \tag{1}$$
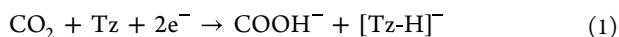
The first step of reaction 1 can be either the reduction of CO_2 or Tz or the formation of the RC (Figure 1a) via C−N bond

a. Path I
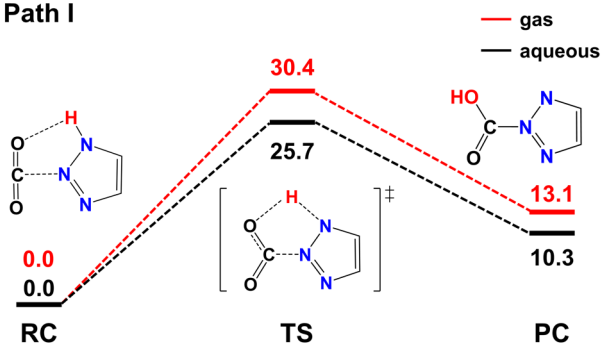
b. Path II

Figure 1. Potential energy profile of the proton transfer step of CO_2 reacting with 1-H-Tz for paths I and II. Method: DLPNO−CCSD(T)/aug-cc-pVTZ//M06-2X/6-31+G(d,p).

formation. Under the aqueous phase, direct reduction of CO_2 or Tz requires a reduction potential E_{red} (vs SHE) of −1.90[61] or −2.99 V (Table S3). Albeit the value of E_{red} is negative (i.e., difficult to reduce), on the one hand, simulations suggested that the redox potential of molecules at the air−water interface could be modified; on the other hand, experiments have shown that spraying pure water into CO_2 gas gives rise to trace amounts of formate anions[24] and spraying Tz-containing water in air gives rise to trace amounts of Tz^- anions.[28] These phenomena confirmed the high redox capability at the air−water interface of the aqueous microdroplet. Notably, spraying Tz-containing water into CO_2 gas greatly improved the amount of formate anions generated, indicating the promoting role of Tz. Calculation indicates the favorable binding of CO_2 to Tz ($\Delta E_{binding}$ = −4.7 kcal/mol, Table S4), thus driving the conversion that follows.

Upon the binding of CO_2 and Tz to form the RC, this complex can follow two paths. For path I (Figure 1a), the system first crosses a proton transfer transition state (TS) at a barrier height of 25.7 kcal/mol and generates the product complex (PC), which subsequently takes one-electron reduction to form PC^-. For path II, the RC first takes one-electron reduction and then crosses the proton transfer barrier (TS^-, 15.7 kcal/mol) and forms PC^- (Figure 1b). The reduction potentials of the RC (−1.87 V) and PC (−1.86 V) are similar to each other and to that of CO_2, indicating that the electron generated at the air−

water interface can be harnessed to reduce the RC or PC. Further reduction of RC^-/PC^- is difficult with E_{red} values of −2.07 or −2.87 V, respectively. On the contrary, the step of $PC^- + e^- \rightarrow COOH^- + [Tz\text{-}H]^-$ (E_{red} = −0.13 V) is relatively easy to occur, indicating that the simultaneous reduction of PC^- and breaking of the C−N bond is possible to generate $COOH^-$. Note that PC^- was not observed in the mass spectrum, confirming its fast conversion.

It was experimentally found that the ●COOH radical was captured during the reaction of spraying Tz/water in microdroplets surrounded by CO_2.[28] We speculate that ●COOH can be formed from PC^-. This is supported by the calculation that in the aqueous phase breaking the C−N bond of PC^- to generate ●COOH and $[Tz\text{-}H]^-$ is only 6.8 kcal/mol uphill. Alternatively, the H● radical may participate in the process, for the reaction $OH^- + H_3O^+ \rightarrow \bullet OH + H\bullet + H_2O$ is spontaneous in the gas phase (ΔG = −117.1 kcal/mol) and is possible at the surface of a water droplet (estimated to be −21.6 kcal/mol, Table 1). There are both direct and indirect pieces of experimental evidence confirming the existence of H● and ●OH radicals at the surface of the water microdroplets.[25,26,60,62−66] So, the association of CO_2 and H● to form ●COOH was checked and was found to be possible. The calculated association energy was −6.3 kcal/mol in the aqueous phase and 3.6 kcal/mol in the gas phase. Furthermore, a free radical scavenger, (2,2,6,6-tetramethylpiperidin-1-yl)oxyl (TEMPO), was employed in the spraying of water microdroplets surrounded by CO_2. The ●COOH radical and dimer radical (●COOH + HCOOH) were successfully captured in the form of ions at m/z 202 ([TEMPO−COOH + H]⁺) and m/z 248 ([TEMPO−COOH + FA + H]⁺), respectively (Figure 2). Similarly, the RC can bind to H● and generate ●COOH, with a free energy of reaction RC + H● → ●COOH + Tz of −0.6/−9.8 kcal/mol in the gas/aqueous phase.
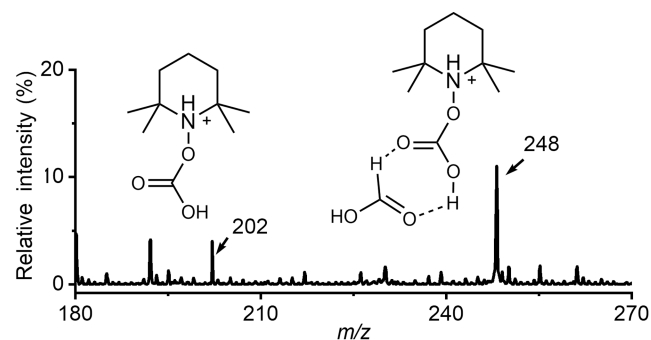
Figure 2. Mass spectrum of spraying water microdroplets containing TEMPO surrounded by CO_2.

One may ask whether CO_2 can grab a proton from water and then gain an electron to form ●COOH. For example, Huang et al. proposed that CO_2 can be protonated by the superacid at a water/CH_3CN microdroplet interface and accelerate the reaction with an amine.[24,67,68] Therefore, we computed the protonation energy of $CO_2 + H_3O^+ \rightarrow COOH^+ + H_2O$. We found the value is as high as 34.1 and 39.5 kcal/mol in the gas phase and aqueous phase, respectively. This result indicates that a super acidic environment is required for the reaction to happen in the bulk solution; thus, under the experimental condition of pH = 5 to 6,[28] direct protonation of CO_2 is prohibited.

Further, we examined the possibility of protonation of Tz by H_3O^+. This protonation step is exothermic in the aqueous phase (−6.2 kcal/mol) and gas phase (−36.1 kcal/mol). Then, the

protonated Tz encounters a barrier of 35.3 (aqueous) or 33.2 (gas) kcal/mol as it transfers a proton to CO_2 (Figure S1), much higher than path I and II. So, direct protonation of Tz is also unlikely to promote further CO_2 conversion. These calculations are in line with the experimental observation that no $COOH^-$ was observed at pH = 4.[28]

In brief, calculations suggest that at the surface of the water microdroplet, multiple ways lead to the formation of the ●COOH radical, association of CO_2 and H●, reduction of CO_2 followed by protonation, and the association of RC and H● followed by the breaking of the C–N bond. In the presence of Tz, the initial step is most likely to be the formation of the RC between CO_2 and Tz. For this step, now that the reduction steps are proven to be feasible, the limiting step for reaction 1 becomes the proton transfer (PT) step for both paths I and II. The PT barrier is smaller for path II (15.7 kcal/mol) than for path I (25.7 kcal/mol), indicating path II is favored. Next, we explore the effect of partial solvation, interfacial electric field, and explicit solvent molecules on this PT step.

Partial Solvation. As the reaction moves from the aqueous phase to the gas phase, the PT barrier increases from 25.7 to 30.4 kcal/mol for path I, whereas it decreases from 15.7 to 6.1 kcal/mol for path II (Table 2). Therefore, when the species are partially solvated at the air–water interface, the proton transfer of RC^- becomes easier, meaning path II will be facilitated.

Table 2. Calculated Barriers of Proton Transfer (PT) for Multiple Mechanisms in the Aqueous (aq.) and Gas Phases

$^a\Delta G^\ddagger$	$^b F_x$	path I		path II	
		aq.	gas	aq.	gas
direct PT	0.0	25.7	30.4	15.7	6.1
one-water bridge PT	0.0	17.9	27.5	12.9	7.7
water-transporter PT	0.0	21.9	46.1	28.3	28.6

^{a}unit in kcal/mol. ^{b}unit in V/Å. Method: DLPNO–CCSD(T)//aug-cc-pVTZ//M06-2X/6-31+G(d,p).

Interfacial Electric Field. The electric field at the surface of the aqueous microdroplet was found to be on the order of 10^9 V/m.[35] It is known that an electrical field oriented along the reaction axis can change the barrier of a reaction that experiences a dipole moment change. Here, we applied a range of electric fields, $F_x = -0.1$ to 0.1 V/Å, along the direction of proton transfer and evaluated the barrier change.

As shown in Figure 3a, a positive F_x of 0.1 V/Å lowers the PT barrier for path I by 3.2 kcal/mol; on the contrary, it raises the PT barrier for path II by 2.1 kcal/mol and vice versa if a negative F_x is applied. This is because the electron transfers in the opposite direction for the PT step of paths I and II (Figure 3b), and our definition of positive F_x promotes the electron transfer of path I, thus lowering the barrier. The x-axis component of dipole moment μ_x increases from the RC ($\mu_x = 1.6$ D) to TS (9.6 D), and the electron transfers from the Tz-side to the CO_2-side. Natural bonding orbital analysis illustrates the donation of electron density from the lone pair of N(Tz) to the π^* orbital of CO_2 (Figure S2a). On the contrary, μ_x decreases from RC^- ($\mu_x = 12.1$ D) to TS^- (7.4 D), and the electron transfers from the CO_2^--side to the Tz-side. This is because in path II, upon the injection of an electron into the RC, the CO_2-moiety is reduced and the electron occupies the π^* antibonding orbital, leading to a bent CO_2 structure in RC^-. Then, as the proton transfers from
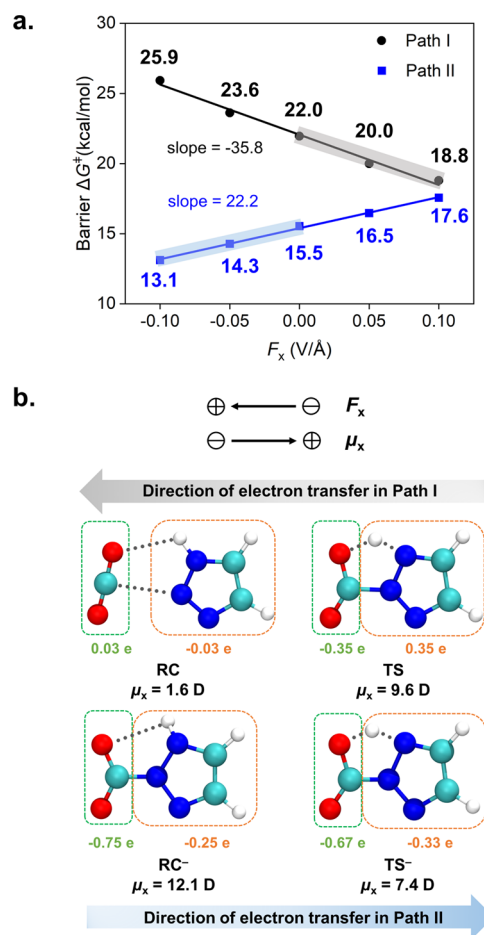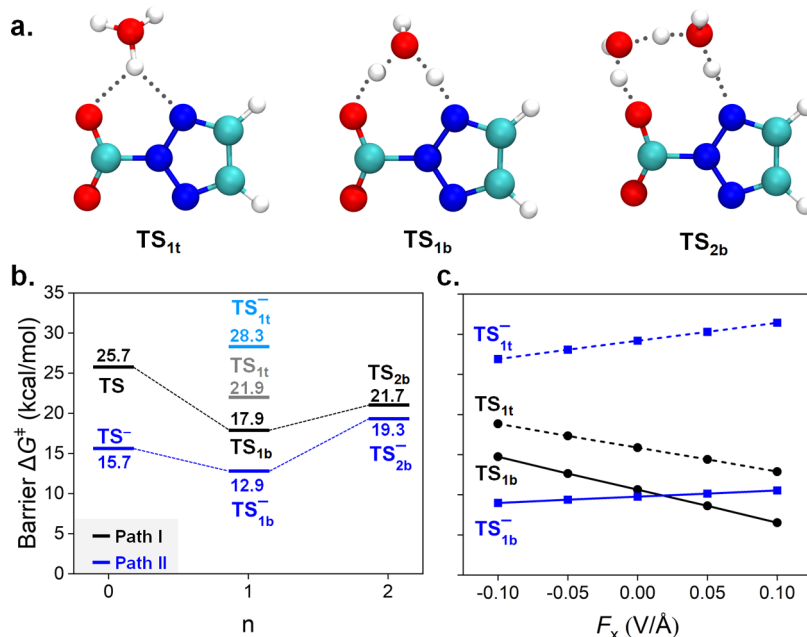

Figure 3. (a) Proton transfer barrier as a function of applied electric field F_x for paths I and II. (b) Dipole moment μ_x and Mulliken charges of RC, TS, RC^-, and TS^-, with directions of F_x, μ_x, and electron transfer illustrated. Method: M06-2X/6-31+G(d,p).

N to O, the electron flows from C to Tz. Mulliken charges are listed in Figure S3.

The opposing trend of barrier change under the applied EF also aligns with the dipole moment change along the reaction, $\Delta\mu^\ddagger = \mu_{TS} - \mu_{RC}$. In the presence of a uniform electric field F, the change in energy G of a molecular system is approximately $\Delta G = -\mu F$, where μ is the component of the molecular dipole moment in the direction of the field, and it is μ_x in our case. Hence the barrier change subjected to the electric field is $\Delta\Delta G^\ddagger = \Delta\mu_x^\ddagger \cdot F_x$. Calculations give the value of $\Delta\mu_x^\ddagger$ to be 8.0 D for path I and -4.7 for path II. Consequently, this explains the differential stabilization under the applied EF (Figure S5), which leads to the opposite barrier change trend for the two paths. The slope value given by DFT calculation indicates the differential barrier change rate.

It is worth mentioning that the direction of the EF is defined simply for the convenience of discussion. In reality, molecules orient randomly and the electric field can align the molecules to its favorable directions and catalyze the reaction.[69] Therefore, under a 0.1 V/Å electric field, the PT barrier can be lowered by at most 3.2 and 2.4 kcal/mol for paths I and II, respectively.

Water Molecule as a Bridge. Water molecules were known to catalyze atmospheric, biological, and organic chemical reactions by serving as a proton shuttle.[70–73] We found that a one-water bridge can significantly lower the PT barrier of path I (by 7.8 kcal/mol, TS_{1b}) and slightly lower that of path II (by 2.8

Figure 4. (a) Structures of TS_{1t}, TS_{1b}, and TS_{2b}. Proton transfer barrier as a function of (b) number of water molecules n and (c) applied electric field F_x for paths I and II.
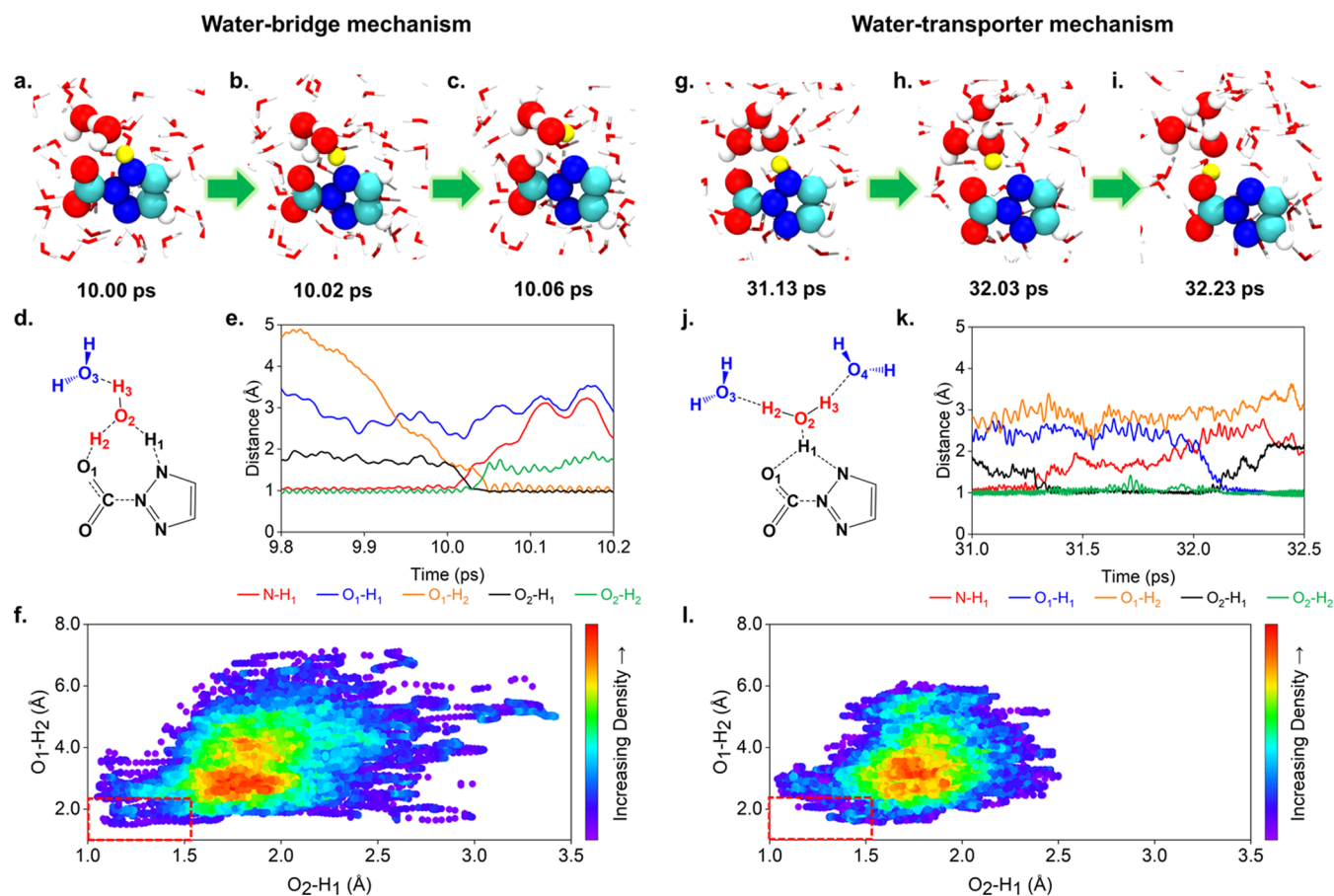
Figure 5. Proton transfer mechanism observed in *ab initio* molecular dynamics simulations at the air−water interface. Snapshots of (a−c) water-bridge mechanism and (g−i) water-transporter mechanism. (d, e), (j, k) Evolution of critical bonds during the trajectories. (f, l) Distribution of configurations before the proton transfer as obtained from representative trajectories.

kcal/mol, TS_{1b}^-). Adding a second water molecule does not further reduce the energy barrier (Figure 4b).

On top of the one- or two-water bridged system, an electric field was applied along the N → C direction as defined in Figure

3. Similarly, a positive F_x lowers (raises) the water-bridged PT barrier of path I (II). In comparison, for path II, the barrier increases more slowly for the water-bridge case (see TS_{1b}^{-} in Figure 4c) than that for the water-free case (see TS^{-} in Figure 3a). As for path I, the barrier-decreasing trend is similar for the water-bridge and water-free cases. These trends are in accord with the dipole moment changes along the reaction coordinates (Table S11).

Taken together, the PT barrier for path I (II) can be reduced by 11.9 (3.6) kcal/mol, where the involvement of one-water bridge contributes 7.8 (2.8) kcal/mol reduction and electric field (0.1 V/Å) contributes 4.1 (0.8) kcal/mol reduction. The resulting PT barrier becomes as low as 6.5 (9.0) kcal/mol for path I (II). Moreover, partial solvation may further reduce the barrier for path II, as discussed above and in Table S12. Thus, at the air−water interface of the microdroplet, both the electric field and water molecule can facilitate the proton transfer step.

Source of Proton. A major difference between direct PT and the water-bridge PT mechanism is the source of proton, which is Tz for the former and water solvent molecules for the latter. Previously,[28] spraying Tz-containing deuterated water microdroplets in CO_2 nebulizing gas generated both $HCOO^{-}$ and $DCOO^{-}$. This observation indicates both Tz and water can be a proton donor. This validates the possibility of the proposed path I and II mechanisms as well as the water-bridge mechanisms.

Noting that the aforementioned DFT calculations neglect the dynamical effect of water molecules, *ab initio* molecular dynamics (AIMD) simulations augmented by the metady-namics-based method were performed for the reaction at the air−water interface. The trajectories were initiated from the RC and the C−N bond was selected as a collective variable (CV). Among the 20 trajectories, both direct PT and water-bridge PT mechanisms were observed at roughly equal probabilities (Table S13).

In terms of the water-bridge PT mechanism, the number of water molecules involved in the bridge can be one, two, or three. We take the one-water bridge case for illustration (Figure 5a−c). The proton transfer from Tz to adjacent O(water) and that from O(water) to $O(CO_2)$ happen simultaneously and are remark-ably fast, within 0.1 ps (Figure 5e). A transient Eigen-like hydronium structure[74] was observed (Figure 5b). Including more water molecules in the water bridge makes the PT steps in sequence and requires a longer time, roughly 0.4−1.0 ps. For instance, when two water molecules serve as the water bridge (Figure S9), H1(Tz) first transfers to O1, followed by the transfer of H2(water) to O2. Then, the system exists in the form of a hydrated hydronium ion for ∼0.4 ps, and finally, H3(water) transfers to $O(CO_2)$ to form the formate group.

In terms of the direct N-to-$O(CO_2)$ PT mechanism, an examination of the trajectories indicates an interesting picture that might have been overlooked before. We found that the closest water molecule behaves like a transporter during the proton transfer, so we named it the water-transporter PT mechanism. As shown in Figure 5g−i, initially, Tz transfers H1 to the closest O2(water) and forms a hydronium anion; then H3(water) fluctuates between two water molecules (i.e., O1 and O2), displaying a Zundel structure.[75] After a period of time (∼0.8 ps), as long as H3 transfers back to O2(water), O2(water) donates H1 to $O(CO_2)$ and forms the COOH-moiety. Therefore, from the perspective of dynamics, the "direct" PT transfer is not so direct, for it is complicated by surrounding water molecules and their proton networks. During this water-
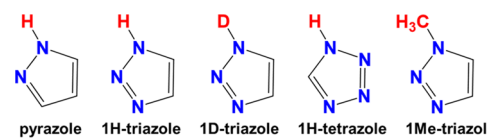
transporter PT process, the O(water)-atom of the transporter water molecule migrates considerably relative to Tz unlike the water-bridge case, where the O(water)-atom barely moves.

Dynamically, the water-bridge mechanism is expected to be faster than the water-transporter mechanism because the latter involves the migration of a heavier O atom. This is reflected in the simulation; an average of ∼0.05 vs ∼0.8 ps was experienced for each respective process (Table S13). At the same time, the water-transporter transition structure (TS_{1t}) is 21.9 kcal/mol higher in energy than the water-bridge transition structure (TS_{1b}) (Table 2 and Figure 4b). The above analysis indicates that the water-transporter mechanism is less favored than the water-bridge mechanism; therefore, it is quite surprising that our simulations give a 1:1 ratio. Checking the trajectories reveals that the hydrogen-bond network of ambient water greatly affects the type of mechanism. If the closest water directs both H atoms to adjacent water molecules (Figure 5g), then the water-transporter mechanism takes place. If the closest water directs one H atom to an adjacent water molecule and the other to the O atom of the CO_2-moiety (Figure 5a), then the water-bridge mechanism takes place. We speculate that the high con-formation distribution of the former configuration could be the driving force of the water-transporter mechanism. Analysis of the trajectories indicates that, before the proton transfer takes place, only a small number of configurations (regions within the red box in Figure 5f,l) resemble the configuration in Figure 5a; while a considerably larger number of configurations (regions above the red box in Figure 5f,l) resemble the configuration in Figure 5g. Furthermore, applying an electric field can also lower the barrier of TS_{1t}. Under F_x = 0.1 V/Å, the barrier drops by 3.0 kcal/mol (Figure 4c).

To our surprise, for path II, the water-transporter mechanism has a much higher barrier, $\Delta G^{\ddagger}(TS_{1t}^{-})$ = 28.3 kcal/mol, than the barrier of the water-free (15.7 kcal/mol) or the water-bridge (12.9 kcal/mol) mechanism. Hence, path II will proceed through the water-free transition structure TS^{-}, for the barrier at the air−water interface lies between 15.7 and 6.1 kcal/mol, and the proton source is Tz.

Multiple Azoles. To examine the validity of the proposed mechanism, we further computed the barrier of other azoles, including pyrazole, tetrazole, 1D-1,2,3-triazole, and 1Me-1,2,3-triazole. As shown in Table 3, except for 1Me-1,2,3-triazole, all of the azoles are capable of proceeding path II, as each barrier is lower than 20 kcal/mol.

Table 3. Proton Transfer Barriers of Multiple Mechanisms for Reaction of CO_2 with Azoles

	path I		path II	
[a] $\Delta G^{\ddagger}$	TS	TS_{1b}	TS^{-}	TS_{1b}^{-}
pyrazole	17.8	12.0	18.6	15.9
1*H*-1,2,3-triazole	25.7	17.9	15.7	12.9
1D-1,2,3-triazole	26.6	18.3	16.7	13.8
1*H*-tetrazole	35.1	28.2	13.5	12.2

[a]unit in kcal/mol. Method: DLPNO−CCSD(T)/aug-cc-pVTZ// M06-2*X*/6-31+G(d,p).

For pyrazole, the path I mechanism can compete with the path II mechanism because the barriers are similar. The respective value is 17.8 vs 18.6 kcal/mol for solvent-free case and 12.0 vs 15.9 kcal/mol for the one-water bridge mechanism. Interestingly, as the reactant changes from pyrazole to triazole to tetrazole, i.e., the number of N atoms increases from 2 to 4, the barrier of path I gradually increases while the barrier of path II gradually decreases. It gives us a hint that varying the number of N atoms in the azole molecule affects the mechanism as it reacts with CO_2 surrounding the water microdroplet. Of note, in the case of methylated tetrazole (1Me-1,2,3-triazole), attempts to locate the transition structures that transfer a proton from methyl to CO_2 were not successful; the corresponding product complex and the products, i.e., $COOH^+ + [1Me\text{-}Tz\text{-}H]^-$, are 65.1 and 113.6 kcal/mol higher in energy than the reactant complex, confirming that this pathway is prohibited. This explains why FA cannot be experimentally detected in water microdroplets containing 1Me-1,2,3-triazole.[28] In fact, methyl transfer from 1Me-1,2,3-triazole to CO_2 is even easier than proton transfer, although the barrier (75.3 kcal/mol) and reaction energy (74.3 kcal/mol) are too high to happen.

■ CONCLUSIONS

By means of quantum chemistry calculations and AIMD simulations, we elucidated the mechanism for converting gas-phase CO_2 to formic acid in a Tz-containing water microdroplet. The air−water interface is critical in promoting the reaction. The CO_2 molecule is first captured by Tz and forms a reactant complex (CO_2-Tz complex, RC) via C−N bonding at the interface of the microdroplet. Then, the RC either proceeds via path I, intramolecular proton transfer followed by reduction, or path II (which is favored), reduction followed by proton transfer, to form the reduced product complex $[HCO_2\text{-}(Tz-H)]^-$, which we call PC$^-$. Subsequently, simultaneous reduction and C−N bond breaking give rise to anionic products $[Tz\text{-}H]^-$ and $COOH^-$, where the latter spontaneously coverts to HCOOH. The properties of water microdroplets effectively facilitate the progression of the reaction. For both paths, the barriers to the proton transfer step are lowered under the condition of an applied electric field that is generated at the air−water interface, as well as lowered via the water-bridge mechanism. These mechanisms were further verified by testing multiple azoles, including pyrazole, 1D-triazole, tetrazole, and 1-Me-triazole to react with CO_2. Aforementioned AIMD simulations at the air−water interface reveal a mechanism that has been overlooked, where the water molecule serves as a transporter and is shown to be favored dynamically.

The transient ●COOH captured by the experiment was proposed to be formed in multiple ways at the surface of the water microdroplet, including association of CO_2 and H●, the association of RC and H● followed by the breaking of the C−N bond, or the dissociation of PC$^-$ to ●COOH and $[Tz\text{-}H]^-$. Considering the trace amount of H●, the latter path is dominant in the presence of Tz.

This work elucidates how multiple factors of microdroplets interplay with each other, thus affecting the kinetics and dynamics of converting CO_2 to formic acid by means of Tz dissolved in water microdroplets at the molecular level. This research holds profound implications for applying microdroplet chemistry in synthesis and for advancing sustainable chemistry and green technology.

■ ASSOCIATED CONTENT

Ⓢ Supporting Information

The Supporting Information is available free of charge at https://pubs.acs.org/doi/10.1021/jacs.4c00529.

> Additional details on the benchmark studies; quantum chemical calculations on mechanisms of 1H-1,2,3-triazole and 2H-1,2,3-triazole; ab initio molecular dynamics simulations (AIMD); original data in calculations. (PDF)

One water bridge (MP4)
Two water bridge (MP4)
Three water bridge (MP4)
Water transport (MP4)
Coordinates (XYZ)

■ AUTHOR INFORMATION

Corresponding Authors

Richard N. Zare − *Department of Chemistry, Stanford University, Stanford, California 94305, United States;* ⓘ orcid.org/0000-0001-5266-4253; Email: zare@stanford.edu

Jing Xie − *Key Laboratory of Cluster Science of Ministry of Education, Beijing Key Laboratory of Photoelectronic/Electrophotonic Conversion Materials, School of Chemistry and Chemical Engineering, Beijing Institute of Technology, Beijing 100081, China;* ⓘ orcid.org/0000-0001-9676-5734; Email: jingxie@bit.edu.cn

Authors

Ke Gong − *Key Laboratory of Cluster Science of Ministry of Education, Beijing Key Laboratory of Photoelectronic/Electrophotonic Conversion Materials, School of Chemistry and Chemical Engineering, Beijing Institute of Technology, Beijing 100081, China*

Yifan Meng − *Department of Chemistry, Stanford University, Stanford, California 94305, United States;* ⓘ orcid.org/0000-0001-6897-3595

Complete contact information is available at:
https://pubs.acs.org/10.1021/jacs.4c00529

Author Contributions

§K.G. and Y. M. contributed equally to this work.

Notes

The authors declare no competing financial interest.

■ ACKNOWLEDGMENTS

■ REFERENCES

(1) Asiri, A. M.; Lichtfouse, E. *Conversion of Carbon Dioxide Into Hydrocarbons Vol. 2 Technology*; Springer, 2020.

G

(2) Behr, A.; Nowakowski, K. Catalytic Hydrogenation of Carbon Dioxide to Formic Acid. In *Advances in Inorganic Chemistry*; Elsevier, 2014; Vol. 66, pp 223−258.

(3) Moret, S.; Dyson, P. J.; Laurenczy, G. Direct synthesis of formic acid from carbon dioxide by hydrogenation in acidic media. *Nat. Commun.* **2014**, 5 (1), No. 4017.

(4) Enthaler, S.; von Langermann, J.; Schmidt, T. Carbon dioxide and formic acid—the couple for environmental-friendly hydrogen storage? *Energy Environ. Sci.* **2010**, 3 (9), 1207−1217.

(5) Ahn, S.; Park, K.; Lee, K. R.; Haider, A.; Van Nguyen, C.; Jin, H.; Yoo, S. J.; Yoon, S.; Jung, K.-D. Atomically dispersed Ru (III) on N-doped mesoporous carbon hollow spheres as catalysts for CO_2 hydrogenation to formate. *Chem. Eng. J.* **2022**, 442, No. 136185.

(6) Estes, D. P.; Leutzsch, M.; Schubert, L.; Bordet, A.; Leitner, W. Effect of ligand electronics on the reversible catalytic hydrogenation of CO_2 to formic acid using ruthenium polyhydride complexes: A thermodynamic and kinetic study. *ACS Catal.* **2020**, 10 (5), 2990−2998.

(7) Jaleel, A.; Haider, A.; Van Nguyen, C.; Lee, K. R.; Choung, S.; Han, J. W.; Baek, S.-H.; Shin, C.-H.; Jung, K.-D. Structural effect of Nitrogen/Carbon on the stability of anchored Ru catalysts for CO_2 hydrogenation to formate. *Chem. Eng. J.* **2022**, 433, No. 133571.

(8) Weilhard, A.; Qadir, M. I.; Sans, V.; Dupont, J. Selective CO_2 hydrogenation to formic acid with multifunctional ionic liquids. *ACS Catal.* **2018**, 8 (3), 1628−1634.

(9) Hori, Y.; Wakebe, H.; Tsukamoto, T.; Koga, O. Electrocatalytic process of CO selectivity in electrochemical reduction of CO_2 at metal electrodes in aqueous media. *Electrochim. Acta* **1994**, 39 (11−12), 1833−1839.

(10) Kang, P.; Zhang, S.; Meyer, T. J.; Brookhart, M. Rapid selective electrocatalytic reduction of carbon dioxide to formate by an iridium pincer catalyst immobilized on carbon nanotube electrodes. *Angew. Chem., Int. Ed.* **2014**, 53 (33), 8709−8713.

(11) Kortlever, R.; Peters, I.; Koper, S.; Koper, M. T. Electrochemical CO_2 reduction to formic acid at low overpotential and with high faradaic efficiency on carbon-supported bimetallic Pd−Pt nano-particles. *ACS Catal.* **2015**, 5 (7), 3916−3923.

(12) Lu, X.; Leung, D. Y.; Wang, H.; Leung, M. K.; Xuan, J. Electrochemical reduction of carbon dioxide to formic acid. *ChemElectroChem* **2014**, 1 (5), 836−849.

(13) Zhu, Q.; Ma, J.; Kang, X.; Sun, X.; Liu, H.; Hu, J.; Liu, Z.; Han, B. Efficient reduction of CO_2 into formic acid on a lead or tin electrode using an ionic liquid catholyte mixture. *Angew. Chem., Int. Ed.* **2016**, 55 (31), 9012−9016.

(14) Albo, J.; Alvarez-Guerra, M.; Castaño, P.; Irabien, A. Towards the electrochemical conversion of carbon dioxide into methanol. *Green Chem.* **2015**, 17 (4), 2304−2324.

(15) Jones, J. P.; Prakash, G. S.; Olah, G. A. Electrochemical CO_2 reduction: recent advances and current trends. *Isr. J. Chem.* **2014**, 54 (10), 1451−1466.

(16) Yang, N.; Waldvogel, S. R.; Jiang, X. Electrochemistry of carbon dioxide on carbon electrodes. *ACS Appl. Mater. Interfaces* **2016**, 8 (42), 28357−28371.

(17) Zhu, D. D.; Liu, J. L.; Qiao, S. Z. Recent advances in inorganic heterogeneous electrocatalysts for reduction of carbon dioxide. *Adv. Mater.* **2016**, 28 (18), 3423−3452.

(18) Rao, H.; Schmidt, L. C.; Bonin, J.; Robert, M. Visible-light-driven methane formation from CO_2 with a molecular iron catalyst. *Nature* **2017**, 548 (7665), 74−77.

(19) Sahara, G.; Ishitani, O. Efficient photocatalysts for CO_2 reduction. *Inorg. Chem.* **2015**, 54 (11), 5096−5104.

(20) Takeda, H.; Cometto, C.; Ishitani, O.; Robert, M. Electrons, photons, protons and earth-abundant metal complexes for molecular catalysis of CO_2 reduction. *ACS Catal.* **2017**, 7 (1), 70−88.

(21) Gong, C.; Li, D.; Li, X.; Zhang, D.; Xing, D.; Zhao, L.; Yuan, X.; Zhang, X. Spontaneous reduction-induced degradation of viologen compounds in water microdroplets and its inhibition by host−guest complexation. *J. Am. Chem. Soc.* **2022**, 144 (8), 3510−3516.

(22) Huang, K.-H.; Wei, Z.; Cooks, R. G. Accelerated reactions of amines with carbon dioxide driven by superacid at the microdroplet interface. *Chem. Sci.* **2021**, 12 (6), 2242−2250.

(23) Kumar, A.; Mondal, S.; Sandeep; Venugopalan, P.; Kumar, A.; Banerjee, S. Destabilized carbocations caged in water microdroplets: Isolation and real-time detection of α-carbonyl cation intermediates. *J. Am. Chem. Soc.* **2022**, 144 (8), 3347−3352.

(24) Qiu, L.; Cooks, R. G. Simultaneous and spontaneous oxidation and reduction in microdroplets by the water radical cation/anion pair. *Angew. Chem.* **2022**, 134 (41), No. e202210765.

(25) Xing, D.; Meng, Y.; Yuan, X.; Jin, S.; Song, X.; Zare, R. N.; Zhang, X. Capture of Hydroxyl Radicals by Hydronium Cations in Water Microdroplets. *Angew. Chem., Int. Ed.* **2022**, 61 (33), No. e202207587.

(26) Zhang, D.; Yuan, X.; Gong, C.; Zhang, X. High Electric Field on Water Microdroplets Catalyzes Spontaneous and Ultrafast Oxidative C−H/N−H Cross-Coupling. *J. Am. Chem. Soc.* **2022**, 144 (35), 16184−16190.

(27) Zhao, P.; Gunawardena, H. P.; Zhong, X.; Zare, R. N.; Chen, H. Microdroplet ultrafast reactions speed antibody characterization. *Anal. Chem.* **2021**, 93 (8), 3997−4005.

(28) Song, X.; Meng, Y.; Zare, R. N. Spraying Water Microdroplets Containing 1,2,3-Triazole Converts Carbon Dioxide into Formic Acid. *J. Am. Chem. Soc.* **2022**, 144 (37), 16744−16748.

(29) Jin, S.; Chen, H.; Yuan, X.; Xing, D.; Wang, R.; Zhao, L.; Zhang, D.; Gong, C.; Zhu, C.; Gao, X.; Chen, Y.; Zhang, X. The Spontaneous Electron-Mediated Redox Processes on Sprayed Water Microdroplets. *JACS Au* **2023**, 3 (6), 1563−1571.

(30) Qiu, L.; Wei, Z.; Nie, H.; Cooks, R. G. Reaction acceleration promoted by partial solvation at the gas/solution interface. *ChemPlusChem* **2021**, 86 (10), 1362−1365.

(31) Wei, Z.; Li, Y.; Cooks, R. G.; Yan, X. Accelerated reaction kinetics in microdroplets: Overview and recent developments. *Annu. Rev. Phys. Chem.* **2020**, 71 (1), 31−51.

(32) Wei, H.; Vejerano, E. P.; Leng, W.; Huang, Q.; Willner, M. R.; Marr, L. C.; Vikesland, P. J. Aerosol microdroplets exhibit a stable pH gradient. *Proc. Natl. Acad. Sci. U.S.A.* **2018**, 115 (28), 7272−7277.

(33) Chamberlayne, C. F.; Zare, R. N. Simple model for the electric field and spatial distribution of ions in a microdroplet. *J. Chem. Phys.* **2020**, 152 (18), No. 184702.

(34) Song, Z.; Liang, C.; Gong, K.; Zhao, S.; Yuan, X.; Zhang, X.; Xie, J. Harnessing the High Interfacial Electric Fields on Water Micro-droplets to Accelerate Menshutkin Reactions. *J. Am. Chem. Soc.* **2023**, 145 (48), 26003−26008.

(35) Xiong, H.; Lee, J. K.; Zare, R. N.; Min, W. Strong electric field observed at the interface of aqueous microdroplets. *J. Phys. Chem. Lett.* **2020**, 11 (17), 7423−7428.

(36) Zhu, C.; Pham, L. N.; Yuan, X.; Ouyang, H.; Coote, M. L.; Zhang, X. High Electric Fields on Water Microdroplets Catalyze Spontaneous and Fast Reactions in Halogen-Bond Complexes. *J. Am. Chem. Soc.* **2023**, 145 (39), 21207−21212.

(37) Inoue, K.-i.; Ahmed, M.; Nihonyanagi, S.; Tahara, T. Reorientation-induced relaxation of free OH at the air/water interface revealed by ultrafast heterodyne-detected nonlinear spectroscopy. *Nat. Commun.* **2020**, 11 (1), No. 5344.

(38) Medders, G. R.; Paesani, F. Dissecting the molecular structure of the air/water interface from quantum simulations of the sum-frequency generation spectrum. *J. Am. Chem. Soc.* **2016**, 138 (11), 3912−3919.

(39) Zhou, Z.; Yan, X.; Lai, Y.-H.; Zare, R. N. Fluorescence polarization anisotropy in microdroplets. *J. Phys. Chem. Lett.* **2018**, 9 (11), 2928−2932.

(40) Rovelli, G.; Jacobs, M. I.; Willis, M. D.; Rapf, R. J.; Prophet, A. M.; Wilson, K. R. A critical analysis of electrospray techniques for the determination of accelerated rates and mechanisms of chemical reactions in droplets. *Chem. Sci.* **2020**, 11 (48), 13026−13043.

(41) Chen, H.; Wang, R.; Xu, J.; Yuan, X.; Zhang, D.; Zhu, Z.; Marshall, M.; Bowen, K.; Zhang, X. Spontaneous Reduction by One Electron on Water Microdroplets Facilitates Direct Carboxylation with CO_2. *J. Am. Chem. Soc.* **2023**, 145 (4), 2647−2652.

(42) Zhao, L.; Song, X.; Gong, C.; Zhang, D.; Wang, R.; Zare, R. N.; Zhang, X. Sprayed water microdroplets containing dissolved pyridine spontaneously generate pyridyl anions. *Proc. Natl. Acad. Sci. U.S.A.* **2022**, *119* (12), No. e2200991119.

(43) Zhao, Y.; Truhlar, D. G. The M06 suite of density functionals for main group thermochemistry, thermochemical kinetics, noncovalent interactions, excited states, and transition elements: two new functionals and systematic testing of four M06-class functionals and 12 other functionals. *Theor. Chem. Acc.* **2008**, *120* (1), 215−241.

(44) Clark, T.; Chandrasekhar, J.; Spitznagel, G. W.; Schleyer, P. V. R. Efficient diffuse function-augmented basis sets for anion calculations. III. The 3-21+G basis set for first-row elements, Li-F. *J. Comput. Chem.* **1983**, *4* (3), 294−301.

(45) Ditchfield, R.; Hehre, W. J.; Pople, J. A. Self-Consistent Molecular-Orbital Methods. IX. An Extended Gaussian-Type Basis for Molecular-Orbital Studies of Organic Molecules. *J. Chem. Phys.* **1971**, *54* (2), 724−728.

(46) Feller, D. The role of databases in support of computational chemistry calculations. *J. Comput. Chem.* **1996**, *17* (13), 1571−1586.

(47) Hariharan, P. C.; Pople, J. A. The influence of polarization functions on molecular orbital hydrogenation energies. *Theor. Chim. Acta* **1973**, *28* (3), 213−222.

(48) Hehre, W. J.; Ditchfield, R.; Pople, J. A. Self-Consistent Molecular Orbital Methods. XII. Further Extensions of Gaussian-Type Basis Sets for Use in Molecular Orbital Studies of Organic Molecules. *J. Chem. Phys.* **1972**, *56* (5), 2257−2261.

(49) Pritchard, B. P.; Altarawy, D.; Didier, B.; Gibsom, T. D.; Windus, T. L. A New Basis Set Exchange: An Open, Up-to-date Resource for the Molecular Sciences Community. *J. Chem. Inf. Model.* **2019**, *59* (11), 4814−4820, DOI: 10.1021/acs.jcim.9b00725.

(50) Schuchardt, K. L.; Didier, B. T.; Elsethagen, T.; Sun, L.; Gurumoorthi, V.; Chase, J.; Li, J.; Windus, T. L. Basis Set Exchange: A Community Database for Computational Sciences. *J. Chem. Inf. Model.* **2007**, *47* (3), 1045−1052.

(51) Guo, Y.; Riplinger, C.; Becker, U.; Liakos, D. G.; Minenkov, Y.; Cavallo, L.; Neese, F. Communication: An improved linear scaling perturbative triples correction for the domain based local pair-natural orbital based singles and doubles coupled cluster method [DLPNO-CCSD (T)]. *J. Chem. Phys.* **2018**, *148* (1), No. 011101.

(52) Neese, F. The ORCA program system. *WIREs Comput. Mol. Sci.* **2012**, *2* (1), 73−78.

(53) Riplinger, C.; Sandhoefer, B.; Hansen, A.; Neese, F. Natural triple excitations in local coupled cluster calculations with pair natural orbitals. *J. Chem. Phys.* **2013**, *139* (13), No. 134101.

(54) Marenich, A. V.; Cramer, C. J.; Truhlar, D. G. Universal solvation model based on solute electron density and on a continuum model of the solvent defined by the bulk dielectric constant and atomic surface tensions. *J. Phys. Chem. B* **2009**, *113* (18), 6378−6396.

(55) Trasatti, S. The absolute electrode potential: an explanatory note (Recommendations 1986). *Pure Appl. Chem.* **1986**, *58* (7), 955−966.

(56) Neese, F. Software update: The ORCA program system—Version 5.0. *WIREs Comput. Mol. Sci.* **2022**, *12* (5), No. e1606.

(57) Frisch, M.; Trucks, G.; Schlegel, H.; Scuseria, G.; Robb, M.; Cheeseman, J.; Scalmani, G.; Barone, V.; Petersson, G.; Nakatsuji, H. *Gaussian 16*, Revision A. 03; Gaussian. Inc.: Wallingford CT, 2016.

(58) Kühne, T. D.; Iannuzzi, M.; Del Ben, M.; Rybkin, V. V.; Seewald, P.; Stein, F.; Laino, T.; Khaliullin, R. Z.; Schütt, O.; Schiffmann, F.; Golze, D.; Wilhelm, J.; Chulkov, S.; Bani-Hashemian, M. H.; Weber, V.; Borštnik, U.; Taillefumier, M.; Jakobovits, A. S.; Lazzaro, A.; Pabst, H.; Müller, T.; Schade, R.; Guidon, M.; Andermatt, S.; Holmberg, N.; Schenter, G. K.; Hehn, A.; Bussy, A.; Belleflamme, F.; Tabacchi, G.; Glöß, A.; Lass, M.; Bethune, I.; Mundy, C. J.; Plessl, C.; Watkins, M.; VandeVondele, J.; Krack, M.; Hutter, J. CP2K: An electronic structure and molecular dynamics software package - Quickstep: Efficient and accurate electronic structure calculations. *J. Chem. Phys.* **2020**, *152* (19), No. 194103.

(59) Fang, Y.-G.; Li, X.; Gao, Y.; Cui, Y.-H.; Francisco, J. S.; Zhu, C.; Fang, W.-H. Efficient exploration of complex free energy landscapes by stepwise multi-subphase space metadynamics. *J. Chem. Phys.* **2022**, *157* (21), No. 214111.

(60) Mehrgardi, M. A.; Mofidfar, M.; Zare, R. N. Sprayed Water Microdroplets Are Able to Generate Hydrogen Peroxide Spontaneously. *J. Am. Chem. Soc.* **2022**, *144* (17), 7606−7609.

(61) Koppenol, W. H.; Rush, J. D. Reduction potential of the carbon dioxide/carbon dioxide radical anion: a comparison with other C1 radicals. *J. Phys. Chem. A* **1987**, *91* (16), 4429−4430.

(62) Meng, Y.; Gnanamani, E.; Zare, R. N. Direct C(sp3)−N Bond Formation between Toluene and Amine in Water Microdroplets. *J. Am. Chem. Soc.* **2022**, *144* (43), 19709−19713.

(63) Chen, X.; Xia, Y.; Zhang, Z.; Hua, L.; Jia, X.; Wang, F.; Zare, R. N. Hydrocarbon Degradation by Contact with Anoxic Water Microdroplets. *J. Am. Chem. Soc.* **2023**, *145* (39), 21538−21545.

(64) Li, J.; Xia, Y.; Song, X.; Chen, B.; Zare, R. N. Continuous ammonia synthesis from water and nitrogen via contact electrification. *Proc. Natl. Acad. Sci. U.S.A.* **2024**, *121* (4), No. e2318408121.

(65) Lee, J. K.; Walker, K. L.; Han, H. S.; Kang, J.; Prinz, F. B.; Waymouth, R. M.; Nam, H. G.; Zare, R. N. Spontaneous generation of hydrogen peroxide from aqueous microdroplets. *Proc. Natl. Acad. Sci. U.S.A.* **2019**, *116* (39), 19294−19298.

(66) Song, X.; Basheer, C.; Zare, R. N. Water Microdroplets-Initiated Methane Oxidation. *J. Am. Chem. Soc.* **2023**, *145* (50), 27198−27204.

(67) Basuri, P.; Gonzalez, L. E.; Morato, N. M.; Pradeep, T.; Cooks, R. G. Accelerated microdroplet synthesis of benzimidazoles by nucleophilic addition to protonated carboxylic acids. *Chem. Sci.* **2020**, *11* (47), 12686−12694.

(68) Luo, K.; Li, J.; Cao, Y.; Liu, C.; Ge, J.; Chen, H.; Zare, R. N. Reaction of chloroauric acid with histidine in microdroplets yields a catalytic Au−(His)₂ complex. *Chem. Sci.* **2020**, *11* (9), 2558−2565.

(69) Wang, C.; Danovich, D.; Chen, H.; Shaik, S. Oriented external electric fields: Tweezers and catalysts for reactivity in halogen-bond complexes. *J. Am. Chem. Soc.* **2019**, *141* (17), 7122−7136.

(70) Bianco, R.; Hay, P. J.; Hynes, J. T. Theoretical study of O−O single bond formation in the oxidation of water by the ruthenium blue dimer. *J. Phys. Chem. A* **2011**, *115* (27), 8003−8016.

(71) Bonin, J.; Costentin, C.; Robert, M.; Savéant, J.-M.; Tard, C. Hydrogen-bond relays in concerted proton−electron transfers. *Acc. Chem. Res.* **2012**, *45* (3), 372−381.

(72) DuBois, D. L.; Bullock, R. M. Molecular electrocatalysts for the oxidation of hydrogen and the production of hydrogen−the role of pendant amines as proton relays. *Eur. J. Inorg. Chem.* **2011**, *2011* (7), 1017−1027.

(73) Mikulski, R. L.; Silverman, D. N. Proton transfer in catalysis and the role of proton shuttles in carbonic anhydrase. *Biochim. Biophys. Acta, Proteins Proteomics* **2010**, *1804* (2), 422−426.

(74) Wicke, E.; Eigen, M.; Ackermann, T. über den Zustand des Protons (Hydroniumions) in wässriger Lösung. *Z. Phys. Chem.* **1954**, *1* (5−6), 340−364, DOI: 10.1524/zpch.1954.1.5_6.340.

(75) Zundel, G.; Metzger, H. Energiebänder der tunnelnden überschuß-protonen in flüssigen säuren. Eine IR-spektroskopische untersuchung der natur der gruppierungen H₅O₂⁺. *Z. Phys. Chem.* **1968**, *58* (5−6), 225−245.